認できる．

なお本解析では，最大時間刻み幅を1ミリ秒に設定した．自動的な時間刻み幅の制御を取り入れており，規定の反復回数内(7回)でNewton-Raphson反復が収束しない場合は時間刻み幅が半分になるように，また最小反復回数(2回)でNewton-Raphson反復が収束した場合は，時間刻み幅を2倍にするようにしている．ほとんどの時間を1ミリ秒で安定に解析できたが，拍出が最高潮に達する手前と，弁がほとんど閉じかける時は0.5ミリ秒の刻み幅が必要であった．計算性能は，Pentium 4(3 GHz)で1回の拍出につき7時間程度であった．この高速化には，効率の良い強連成計算を可能にする第7節で説明した反復ソルバが大きく貢献している．

9 まとめ

本稿では，従来のFicitious domain法とは異なり，流体構造界面での流速の補間を必要としない制約条件式を，連続の式をもとに構成する方法を提案した．本提案手法の力学的な解釈を試みた結果，導入したラグランジュ未定乗数の畳み込みから得られる関数が，界面における圧力の不連続性を表現するために新たに追加された有限要素法の補間関数とみなせることがわかった．界面での不連続性を表現するための補間関数の追加というアイデアをさらに流体領域が分断されるときの安定化にも適用し，心臓弁の開閉を伴うシミュレーションを弁の両側の大きな圧力差に耐えながら安定に行なうことも可能にした．

以上のように新たに開発した手法に著者らのロバストな反復解法を組み合わせることで，これまで達成されていなかった大動脈弁における一心周期の流体構造連成解析を体循環モデルも考慮して安定に行なうことが出来た．

謝辞

本研究は，(独)科学技術振興機構戦略的創造研究事業(CREST タイプ，医療・創薬のためのマルチスケール・マルチフィジックス心臓シミュレータの開発)のもとで行なわれたものである．本研究において，東京大学新領域創成科学研究科澤田有弘氏，岡田純一氏には，議論に多大な時間を割いていただくとともに，有効な助言を多数いただいた．また，同研究科梅谷信行氏からは，流体解析部の高速・高精度な積分計算ルーチンを提供いただいた．同研究科黒川洋氏には，DKT シェル要素の剛性行列作成に関して，野田隆史氏には大動脈弁のメッシュ生成に関してご協力いただいた．杉浦清了教授には生理学的側面についてご指導いただいた．これらの諸氏に感謝の意を表する．

[参考文献]

[1] Baaijens, F. P. T., A fictitious domain/mortar element method for fluid-structure interaction, Int. J. Numer. Meth. Fluids, 35(2001), 743-761.

[2] Glowinski, R., Pan, T.-W. and Periaux, J., A fictitious domain method for Dirichlet problem and applications, Comput. Methods Appl. Mech. Engrg., 111(1994), 283-303.
[3] De Hart, J., Peters, G. W. M., Schreurs, P. J. G. and Baaijens, F. P. T., A three-dimensional computational analysis of fluid-structure interaction in the aortic valve, Journal of Biomechanics, 36(2003), 103-112.
[4] 久田俊明, 野口裕久, 非線形有限要素法の基礎と応用, 丸善, 東京, 1995.
[5] Saad, Y., Iterative Methods for Sparse Linear Systems, PWS Publishing Company, Boston, 1996.
[6] Washio, T., Hisada, T., Watanabe, H. and Tezduyar, T. E., A robust and efficient iterative linear solver for strongly coupled fluid-structure interaction problems, Comput. Methods Appl. Mech. Engrg., 194(2005), 4027-4047.
[7] Zhang, Q. and Hisada, T., Analysis of fluid-structure interaction problems with structural buckling and large domain changes by ALE finite element method, Comput. Methods Appl. Mech. Engrg., 190(2001), 6341-6357.

[**Abstract**] We introduce a new approach to simulate fluid-structure interaction of the heart valves. Our approach is based on the Lagrange multiplier method, thus similar to the fictitious domain method. However, unlike the existing approaches, we avoid interpolations of the fluid velocity on the interface with the structure, and introduce equations of continuity around the interface as the constraint conditions instead. Through some mathematical considerations based on a weak formulation of the Navier-Stokes equation, we show the validity of the approach. We also introduce another constraint based on the same idea to achieve stability in the analysis of open-close behavior of the heart valves. A couple of simulations of aortic valves are successfully shown.

Mechanisms of destabilization and early termination of spiral wave reentry in the ventricle by a class III antiarrhythmic agent, nifekalant

Masatoshi Yamazaki, Haruo Honjo, Harumichi Nakagawa, Yuko S. Ishiguro, Yusuke Okuno, Mari Amino, Ichiro Sakuma, Kaichiro Kamiya and Itsuo Kodama

Am J Physiol Heart Circ Physiol 292:539-548, 2007. First published Aug 25, 2006;
doi:10.1152/ajpheart.00640.2006

AJP - Heart and Circulatory Physiology publishes original investigations on the physiology of the heart, blood vessels, and lymphatics, including experimental and theoretical studies of cardiovascular function at all levels of organization ranging from the intact animal to the cellular, subcellular, and molecular levels. It is published 12 times a year (monthly) by the American Physiological Society, 9650 Rockville Pike, Bethesda MD 20814-3991. ISSN: 0363-6135, ESSN: 1522-1539. Visit our website at http://www.the-aps.org/.

Am J Physiol Heart Circ Physiol 292: H539–H548, 2007.
First published August 25, 2006; doi:10.1152/ajpheart.00640.2006.

Mechanisms of destabilization and early termination of spiral wave reentry in the ventricle by a class III antiarrhythmic agent, nifekalant

Masatoshi Yamazaki,[1]* Haruo Honjo,[1]* Harumichi Nakagawa,[1] Yuko S. Ishiguro,[1] Yusuke Okuno,[1] Mari Amino,[2] Ichiro Sakuma,[3] Kaichiro Kamiya,[1] and Itsuo Kodama[1]

[1]*Research Institute of Environmental Medicine, Nagoya University, Nagoya;* [2]*Department of Cardiology, Tokai University School of Medicine, Isehara; and* [3]*Graduate School of Technology, The University of Tokyo, Tokyo, Japan*

Submitted 15 June 2006; accepted in final form 18 August 2006

Yamazaki M, Honjo H, Nakagawa H, Ishiguro YS, Okuno Y, Amino M, Sakuma I, Kamiya K, Kodama I. Mechanisms of destabilization and early termination of spiral wave reentry in the ventricle by a class III antiarrhythmic agent, nifekalant. *Am J Physiol Heart Circ Physiol* 292: H539–H548, 2007. First published August 25, 2006; doi:10.1152/ajpheart.00640.2006.—Nifekalant (NF) is a novel class III antiarrhythmic agent that is effective in preventing life-threatening ventricular tachycardia/fibrillation (VT/VF). We investigated mechanisms of destabilization and early termination of spiral-type reentrant VT by NF in a two-dimensional subepicardial myocardial layer of Langendorff-perfused rabbit hearts ($n = 21$) using a high-resolution optical action potential mapping system. During basic stimulation, NF (0.1 μM) caused uniform prolongation of action potential duration (APD) without affecting conduction velocity and an increase of APD restitution slope. VTs induced by direct current stimulation in the presence of NF were of shorter duration (VTs > 30 s: 2/54 NF vs. 19/93 control). During VTs in control (with visible rotors), the wave front chased its own tail with a certain distance (repolarized zone), and they seldom met each other. The average number of phase singularity (PS) points was 1.31 ± 0.14 per 665 ms ($n = 7$). In the presence of NF, the wave front frequently encountered its own tail, causing a transient breakup of the spiral wave or sudden movement of the rotation center (spatial jump of PS). The average number of PS was increased to 1.63 ± 0.22 per 665 ms ($n = 7$, $P < 0.05$) after NF. The mode of spontaneous termination of rotors in control was in most cases (9/10, 90.0%) the result of mutual annihilation of counterrotating wave fronts. With NF, rotors frequently terminated by wave front collision with the atrioventricular groove (12/19, 63.2%) or by trapping the spiral tip in a refractory zone (7/19, 36.8%). Destabilization and early termination of spiral wave reentry induced by NF are the result of a limited proportion of excitable tissue after modulation of repolarization.

potassium channel blocker; optical mapping; ventricular tachycardia

VENTRICULAR TACHYCARDIA/FIBRILLATION (VT/VF) is the major cause of sudden cardiac death. It is generally believed that regardless of the initiating event, spiral- or vortex-type reentrant activity rotating around a functional obstacle (rotor) is the major organization center of VT/VF (3, 22, 25–27). Pharmacological regulation of such rotors is therefore the central task to be achieved for efficient prevention of sudden arrhythmic death (8, 22, 25, 26). Nifekalant hydrochloride (NF) is a new class III antiarrhythmic drug developed in Japan that causes dose-dependent prolongation of action potential duration (APD) in both atrial and ventricular muscle, mainly by reducing the rapid component of the delayed rectifier K^+ current (I_{Kr}) (12, 16, 17), and at higher concentrations, NF has an inhibitory effect on other voltage- and ligand-gated K^+ currents (12, 16). APD prolongation by pharmacological blockade of I_{Kr} renders a certain proarrhythmic propensity known as drug-induced QT prolongation and torsades de pointes, and this potential risk limits the use of class III antiarrhythmic drugs (20). In experimental animals, however, NF has been shown to prevent VT/VF after acute myocardial infarction without compromising hemodynamics (9) and to improve electrical defibrillation efficacy (14). Several clinical studies have shown the usefulness of intravenous NF in the treatment of patients with recurrent VT/VF that is resistant to other antiarrhythmic drugs and direct current (DC) shocks (15, 16).

In a recent optical mapping study to examine the combined effects of NF and lidocaine in a two-dimensional (2D) subepicardial layer of rabbit ventricular myocardium, we have demonstrated that NF (0.5 μM) alone prolongs VT cycle length and causes its early termination in association with destabilization of the spiral wave dynamics (prolongation of functional block line, frequent local conduction block, and extensive meandering) (1). Preliminary experiments with NF at a lower concentration (0.1 μM) also showed analogous modification of spiral wave reentry (10). On the basis of these observations, we speculated that the NF-induced destabilization of spiral wave reentry may be the result of repolarization delay leading to more frequent wave front-tail interactions, but the issue remains to be substantiated. The mechanism of early VT termination was unclear. The present study was designed to clarity the points in similar 2D rabbit ventricular myocardial tissue preparations. Newly developed software to visualize the wave front and tail of optical action potential signals was employed to analyze their interaction. A phase-mapping method was used to quantify the destabilization and to elucidate the mode of termination of rotors. The results revealed that the wave front during VTs in the presence of NF does frequently encounter its own tail, giving rise to transient breakup of spiral wave or sudden movement of the rotation center, and that early VT termination with NF is the result of either wave front collision with the atrioventricular groove or trapping of the spiral tip in a refractory zone.

METHODS

Experimental preparations. The protocol was approved by the Institutional Animal Care and Use Committee at Nagoya University.

* M. Yamazaki and H. Honjo contributed equally to this work.

Address for reprint requests and other correspondence: I. Kodama, Dept. of Cardiovascular Research, Research Institute of Environmental Medicine, Nagoya Univ., Chikusa-ku, Nagoya 464-8601, Japan (e-mail: ikodama@riem.nagoya-u.ac.jp).

The costs of publication of this article were defrayed in part by the payment of page charges. The article must therefore be hereby marked "*advertisement*" in accordance with 18 U.S.C. Section 1734 solely to indicate this fact.

Experiments were performed in vitro on hearts obtained from Japanese White rabbits of both sexes weighing 1.7–2.0 kg. The experimental procedure was described previously in detail (1). In brief, rabbits were anesthetized with pentobarbital sodium (10–15 mg/kg), and the hearts were rapidly removed. The isolated hearts were continuously perfused on a Langendorff apparatus with modified Krebs-Ringer solution equilibrated with 95% O_2-5% CO_2 to maintain pH 7.4 (37°C). Complete atrioventricular block was produced by ligation of the His bundle. We created a 2D epicardial layer of ventricular myocardium by performing a cryoprocedure (1, 10). This model is similar to that reported by Schalij et al. (23) and has an advantage over use of the intact three-dimensional heart to visualize the spiral wave reentry on the epicardial surface. At the end of the experiment, the heart was stained with 2,3,5-triphenyltetrazolium chloride (TTC) and sectioned parallel to the atrioventricular groove, from base to apex, at 2-mm intervals. The surviving myocardium, which was stained deeply with TTC (reservation of dehydrogenase activity), was 1.0 ± 0.2 mm thick (10 hearts).

High-resolution optical mapping. The optical mapping system used in this study was described previously (1). After endocardial freezing, the hearts were stained with a voltage-sensitive dye, di-4-ANEPPS. To minimize motion artifacts, we added 15 mM 2,3-butanedione monoxime (BDM) unless otherwise specified. Bipolar electrograms were recorded through widely spaced electrodes, one at the apex of the left ventricle and the other at the lateral wall of the right ventricle, to monitor the whole ventricular excitations. The signals were filtered from 15 to 1,000 Hz and digitized at 1,000 Hz.

The hearts were illuminated with bluish light-emitting diodes; the emitted fluorescence was recorded with a solid-state image-sensing digital video camera (Fastcam-Ultima 40K; Photron) to acquire 8-bit gray scale images from 256 × 256 sites simultaneously at a speed of 750 frames/s. The images covered the anterolateral surface of the left ventricle and part of the anterior surface of the right ventricle. Each acquisition lasted 10.9 s.

To reveal the signal, we subtracted the background fluorescence from each frame and applied low-pass spatial filtering. The fluorescence signals were inverted and then spatially averaged to reduce noise. Spatial resolution after the low-pass filtering was 0.36–0.48 mm. Isochrone maps were generated from the filtered image. Action potential configuration was analyzed after the application of a five-point median filter to the spatially averaged data (13), and then the data were normalized to the range of the maximum and the minimum values in the respective 1,000-frame sample. A time point at 10% depolarization in the upstroke phase and a time point at 90% repolarization in its repolarization phase were identified for each action potential signal, and their interval was measured as APD at 90% repolarization (APD_{90}). The distribution of APD_{90} values in the recording area was displayed as a color gradient map with 1.33-ms steps, ranging from red (shortest) to blue (longest).

Wave front-tail dynamics during VT were visualized by connecting the 10% depolarization points in the action potential upstrokes as the wave front (red) in the recording area and by connecting the 90% repolarization points as the wave tail (green). We quantified the pattern of wave propagation during VT using the phase-mapping method described by Gray et al. (5). The fluorescence of each pixel at time t, $F(t)$, was plotted against the fluorescence of the same pixel offset by a time interval $\tau = 25$ frames. A cyclic return map of $F(t)$ vs. $F(t - \tau)$ was constructed, allowing a new parameter, phase $\theta(t)$, to be defined as the angle of the coordinate $[F(t), F(t - \tau)]$ around the mean fluorescence for that given pixel, with values between $-\pi$ and π. After the transformation, a new phase $\theta(t)$ movie was produced that included all pixels, in which different phases of the action potential were represented by a continuous color gradient extending from red to purple. Phase singularity (PS) was defined as the point at which all phases converged.

Experimental protocols. Conduction velocity and APD_{90} were measured during constant (S1) stimulation at the center of the left ventricular free wall at basic cycle lengths (BCLs) of 180–800 ms. A monopolar electrode made of platinum wire was used for stimulation. The longitudinal (LD) and transverse directions (TD) of propagation were determined from the activation maps elicited by S1 stimulation (1). Conduction velocity was measured in a central 18 × 18-mm square around the stimulation site, since measurement in the outer periphery would have been hampered by the sharp curvature of the ventricular surface. Conduction velocities in LD and TD were calculated from the slope of a linear least-squares fit of the activation time plotted against the distance. Data from an area very close to the stimulation site (<2 mm) were excluded to minimize the virtual electrode polarization effects.

We used the dynamic pacing method (11) to characterize the APD restitution property. The center of the left ventricular free wall was initially paced at a BCL of 400 ms, and the BCL was progressively shortened in steps of 5–20 ms. A minimum of 30 stimuli were delivered at a given BCL. APD restitution at a site 5 mm from the stimulation site in TD was analyzed. The APD_{90} of the final paced action potential was measured at a BCL with no APD alternans. When APD alternans occurred at a shorter BCL, the pacing was interrupted twice to measure the APD_{90} of both long and short action potential. The BCL was shortened until either a 2:1 block or higher order periodicity occurred. The APD restitution curve was constructed by plotting APD_{90} against the preceding diastolic interval, and the curve was fitted to a single-exponential function (Origin 7.0; Microcal Software, Northampton, MA).

VTs resulting from spiral-type excitation were induced by modified cross-field stimulation. Eighteen S1 stimuli at a BCL of 400 ms were applied to the apex through a pair of contiguous bipolar electrodes. A 10-ms monophasic rectangular pulse of constant voltage (20 V) was generated by a DC power unit and was delivered from the unit through a 6,700-μF capacitor connected to a power MOS-FET switch. A pair of Ag-AgCl paddle electrodes (7 mm in diameter) were placed on the lateral surface of the left and right ventricles for the DC stimulation (S2) to induce electrical field roughly perpendicular to the S1 excitation from the apex to the base (modified cross-field stimulation). The S1-S2 coupling interval was varied at 10-ms steps to apply S2 during the vulnerable window of the final S1 excitation.

Data were obtained before (baseline) and 20–30 min after application of 0.1 μM NF (Nihon Schering, Osaka, Japan). All the experiments were completed within 120 min of perfusion, during which the conduction velocity, APD_{90}, and APD restitution were unchanged (see Supplemental Table 1; the online version of this article contains supplemental data). We confirmed in pilot experiments of four rabbit hearts that the effects of NF (0.1 μM) on the action potential configuration reached a steady state at ~30 min (see Supplemental Table 2). At the end of experiment, the tissues were fixed in 15% formalin and sectioned parallel to the epicardium at a 8-μm interval. The sections were stained with hematoxylin and eosin to examine the fiber orientation in the mapped area.

Statistical analysis. Group data are expressed as means ± SD. Statistical comparisons were performed using two-way ANOVA with Tukey's test, *t*-test, or Mann-Whitney *U*-test when appropriate. Differences were considered significant when the probability value was <0.05.

RESULTS

Conduction velocity and action potential. Conduction properties and action potential configurations were examined in seven hearts during constant stimulation from a center of the left ventricular free wall at a wide range of BCLs (180–800 ms). The isochrones of activation front exhibited a smooth, symmetric, elliptical pattern; the long axis corresponded to the fiber orientation of subepicardial cardiac muscle. In the central 18 × 18-mm square, there was a linear correlation between

activation times and distances in both LD and TD. Conduction velocity in the LD and TD under control conditions was 55.2 ± 4.3 and 23.1 ± 2.1 cm/s, respectively, at a BCL of 800 ms. The values decreased slightly at shorter BCLs and reached 42.4 ± 3.9 and 16.6 ± 0.8 cm/s, respectively, at a BCL of 180 ms. The anisotropic ratio of the velocity was 2.4 to 2.6. NF at 0.1 μM and caused no significant changes in these parameters.

Figure 1*A* shows representative changes in APD in response to NF application. Action potential signals obtained from 16 sites covering an 18 × 18-mm square were superimposed. NF (0.1 μM) caused uniform prolongation of APD at all recording sites. Figure 1*B* summarizes the changes in APD_{90} (average of the values at the 16 sites). NF caused significant prolongation of APD_{90}, and the prolongation was greater at longer BCLs. The dispersion of the APD_{90} values among the 16 recording sites was virtually unaffected (Fig. 1*C*).

Figure 1, *D* and *E*, shows representative data for the APD restitution. The plots of APD_{90} against the diastolic intervals before and after NF (0.1 μM) both fitted single-exponential function well (Fig. 1*E*). The maximal slope after NF (0.90) was much greater than under the control conditions (0.55). The average of the maximum slope values in five hearts increased from 0.48 ± 0.20 in control to 0.70 ± 0.24 after NF ($n = 5$, $P < 0.05$). NF also enhanced the APD alternans at shorter BCLs; the maximum alternans amplitude was increased from 5.8 ± 2.2 ms in control to 12.5 ± 5.5 ms after NF ($n = 5$, $P < 0.05$).

VTs induced by modified cross-field stimulation. VTs were induced in 15 hearts by DC stimulation before (control) and after NF (0.1 μM) application. In controls, 74 of 93 VTs (79.6%) terminated spontaneously within 30 s (nonsustained), whereas the other 19 (20.4%) persisted >30 s (sustained). Forty-six (49.5%) of the 74 nonsustained VTs terminated within 5 s. Of the 54 VTs in the presence of NF, 52 VTs (96.2%) were nonsustained and the 2 other VTs (3.7%) were sustained. Forty-four (81.5%) of the 52 nonsustained VTs terminated within 5 s. Thus VTs induced in the presence of NF (0.1 μM) terminated earlier than in the control conditions. VT cycle length (VTCL) after NF was significantly longer than under the control conditions (188 ± 31 vs. 154 ± 16 ms, $P < 0.05$).

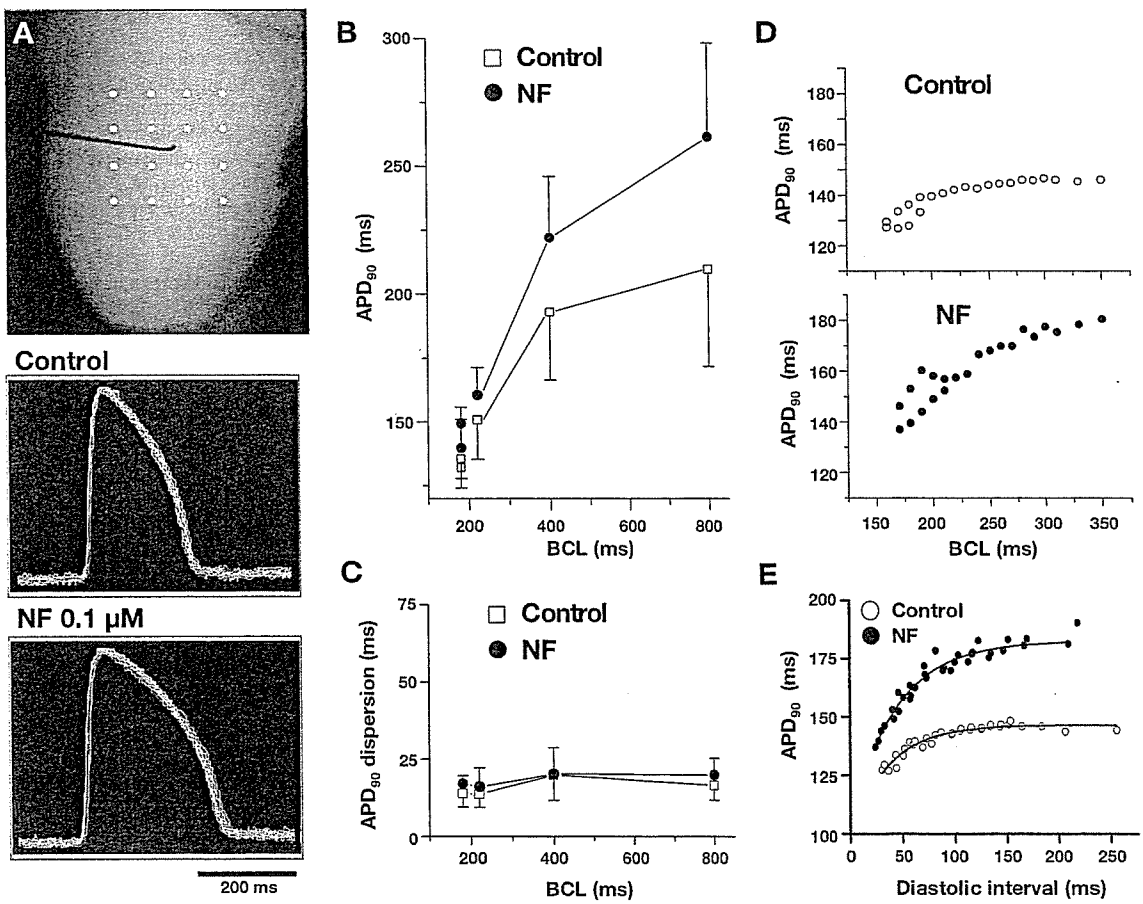

Fig. 1. Action potential duration (APD) and its restitution. *A*, *top*: 16 data-sampling sites (white dots) for APD measurements covering an 18 × 18-mm area around the stimulation site (center of the anterior aspect of the left ventricular free wall). *Bottom*, superimposed action potential signal [at a basic cycle length (BCL) of 800 ms] recorded from the 16 sites before (control) and after application of 0.1 μM nifekalant (NF). *B*: APD at 90% repolarization (APD_{90}) during constant stimulation (average of values at the 16 sites) at a BCL of 180–800 ms before (control) and after NF (means ± SD, $n = 7$). At a BCL of 180 ms, data are presented for long and short APD_{90}, respectively, reflecting alternans. *C*: APD_{90} dispersion among the 16 sites at a BCL of 180–800 ms before (control) and after NF (means ± SD, $n = 7$). *D*: representative relationship between APD_{90} and BCL of dynamic pacing before (control) and after NF. *E*: relationship between APD_{90} and diastolic interval (same experiment as in *D*).

Optical images of excitation during VT were analyzed in nine hearts exhibiting visible rotors in the observation area under the control conditions as well as after NF. Figure 2 shows a representative experiment. The record under the control condition (Fig. 2*A*) was obtained 2 s after VT initiation (see Supplemental Movie 1). Clockwise rotation of wave fronts circulating around a line of functional block (~7 mm) with a VTCL of 141 ms can be seen in isochrone maps. The circuit was more or less stable for >10 s and exhibited minimal meandering. A bipolar electrogram obtained during the VT episode showed monomorphic ventricular excitations. Characteristic features of the action potential configuration around the circuit, which were reported previously (1, 10), are recognized; those include slower upstroke at sites close to the pivot points (*sites b* and *d*), faster upstroke at sites after passing through the pivot points (*sites a* and *c*), clear double potential at the center of functional block line (*site e*), and no isoelectric segments between action potential signals. The block lines (4–9 mm) run either parallel (~70%) or across (~30%) the fiber orientation. There was no obvious tissue damage or macroscopic structural discontinuity to anchor the reentrant pathway in a fixed position.

Figure 2*B* shows the activation pattern during a short VT (lasting for 3 s) induced after application of NF (0.1 μM) (see Supplemental Movie 2). Rotors circulating around functional block lines were observed in isochrone maps during the three consecutive cycles, but their circuits changed dramatically in a beat-to-beat manner, with VTCLs varying from 176 to 195 ms. In *beat 1*, a wave front coming down from the base faced a long oblique functional block line (*site b*), giving rise to its extension toward the right margin. The wave, after turning around the right margin, was divided into dual circuits, one toward the base and another toward the apex and the left margin. The upper circuit showed a local conduction block (*site e*), causing a further extension of the upper block line to maintain the clockwise rotation. In *beat 2*, the clockwise rotation of different dual circuits was preserved; the upper circuit was around a long functional block line in a direction (along the fiber orientation) and configuration similar to those of *beat 1*, whereas the lower circuit was around an L-shaped

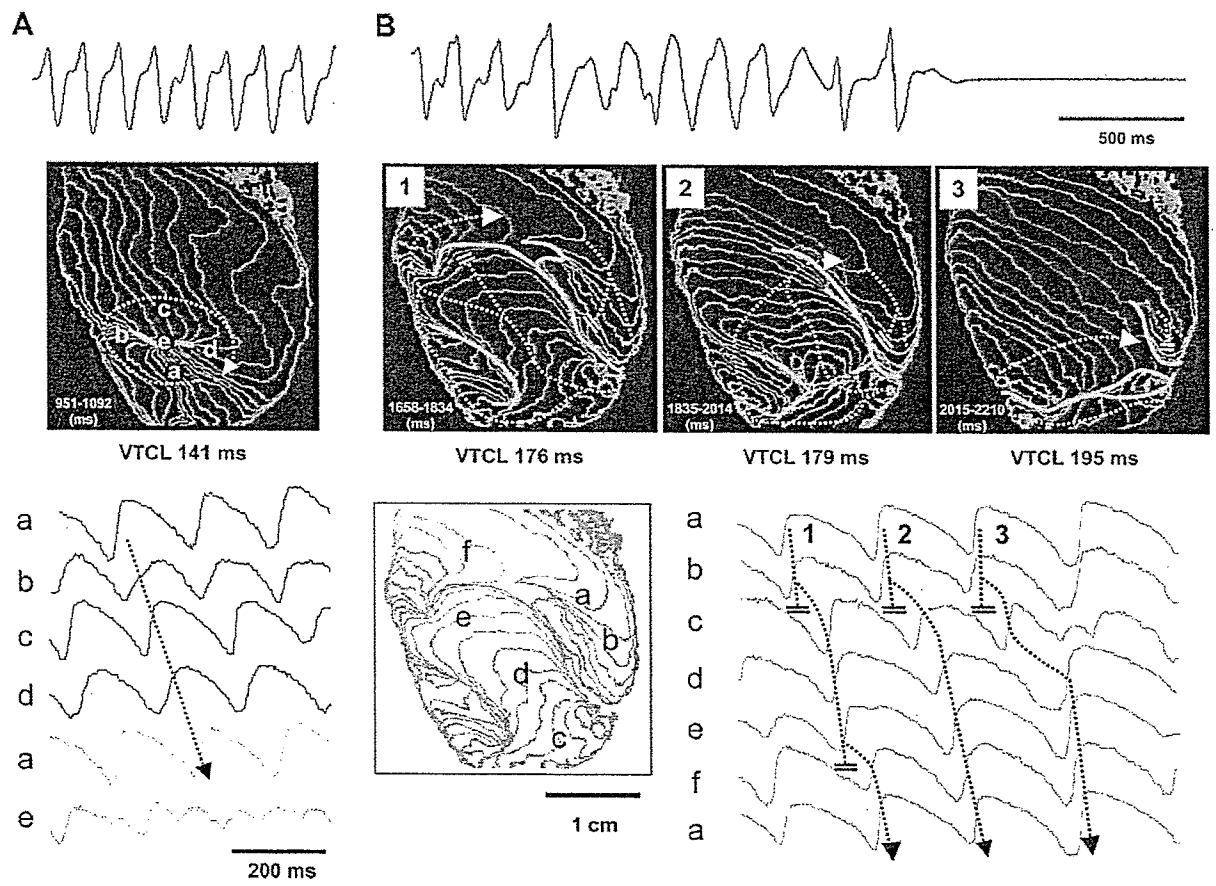

Fig. 2. Spiral wave excitations in the absence and presence of 0.1 μM NF. *A*: ventricular tachycardia (VT) with almost monomorphic configuration under control conditions. A bipolar electrogram obtained during the VT (*top*), an isochrone map (*middle*), and sequential records of 5 optical action potential signals (*bottom*) are shown. Isochrones are 5.33-ms intervals (green lines for earlier wave fronts and blue lines for later wave fronts). Clockwise rotation around a line of block (yellow) in the anterior left ventricular free wall was repeated at a cycle length (VTCL) of 136–141 ms. Optical action potential signals were obtained from 5 sites (*a–e* in the isochrone map). *B*: VT with polymorphic configuration after application of NF. A bipolar electrogram (*top*), isochrone map of *beats 1–3* (*middle*), and sequential records of 6 optical action potential signals (*bottom*) are shown. Clockwise rotation around dual lines of block (yellow) changed their circuits in each excitation with a VTCL of 176–195 ms. Optical action potential signals were obtained from 6 sites (*a–f*) indicated at *left* (isochrone map of *beat 1*). Data in *A* and *B* are from the same heart.

functional block line (one half along and one half across the fiber orientation). In *beat 3*, the upper functional block line moved toward the posterior surface (visible line was shortened). On the other hand, the lower functional block line was largely prolonged, traversing the whole anterior surface. Isochrones in the observation area for *beat 3* showed an almost single large clockwise rotation. The total length of visible functional block lines for the three beats was 23.7–35.2 mm. The rotor terminated spontaneously five cycles later. Bipolar electrograms obtained during the VT episode showed polymorphic torsades de pointes-like ventricular excitations. The action potential signals from the circuits showed a marked beat-to-beat variation that reflects complex meandering of rotors and frequent conduction block.

Qualitatively similar results were obtained in all nine hearts. Thus the characteristic effects of NF on the spiral wave dynamics (prolongation of functional block line, an increase in meandering of circuits, and earlier termination of rotation) (1) have been visualized clearly in experiments at a lower drug concentration (0.1 μM).

Wave front-tail interaction and phase singularity. The mechanisms of NF-induced modification of spiral wave reentry were investigated in terms of the wave front-tail interaction and the PS dynamics. Seven VT episodes with rotors visible in the observation area were analyzed for each before (control) and after application of NF. During VTs under the control conditions, the wave front chased its own tail with a certain distance between them (repolarized zone), and the wave fronts seldom met each other (Fig. 3*A*, *top*). The number of PS points in the phase maps was normally (>90%) 1 (a single rotor; Fig. 3*A*, *bottom*) and, rarely, increased to 2 for a short period (Fig. 3*D*). In the presence of NF (0.1 μM), the wave front frequently encountered its own tail, causing transient breakup of the spiral wave (Fig. 3*B*, *top*) or sudden movement of the organizational center of rotation to another site (Fig. 3*C*, *top*). In the phase maps, the former was recognized as an increase in PS from 1 to 3 (Fig. 3*B*, *bottom*), whereas the latter was recognized as a sudden jump in PS site (Fig. 3*C*, *bottom*). Figure 3*D* shows representative changes in PS number per 500 frames (665 ms) after application of NF. Pooled data are summarized in Fig. 3*E*;

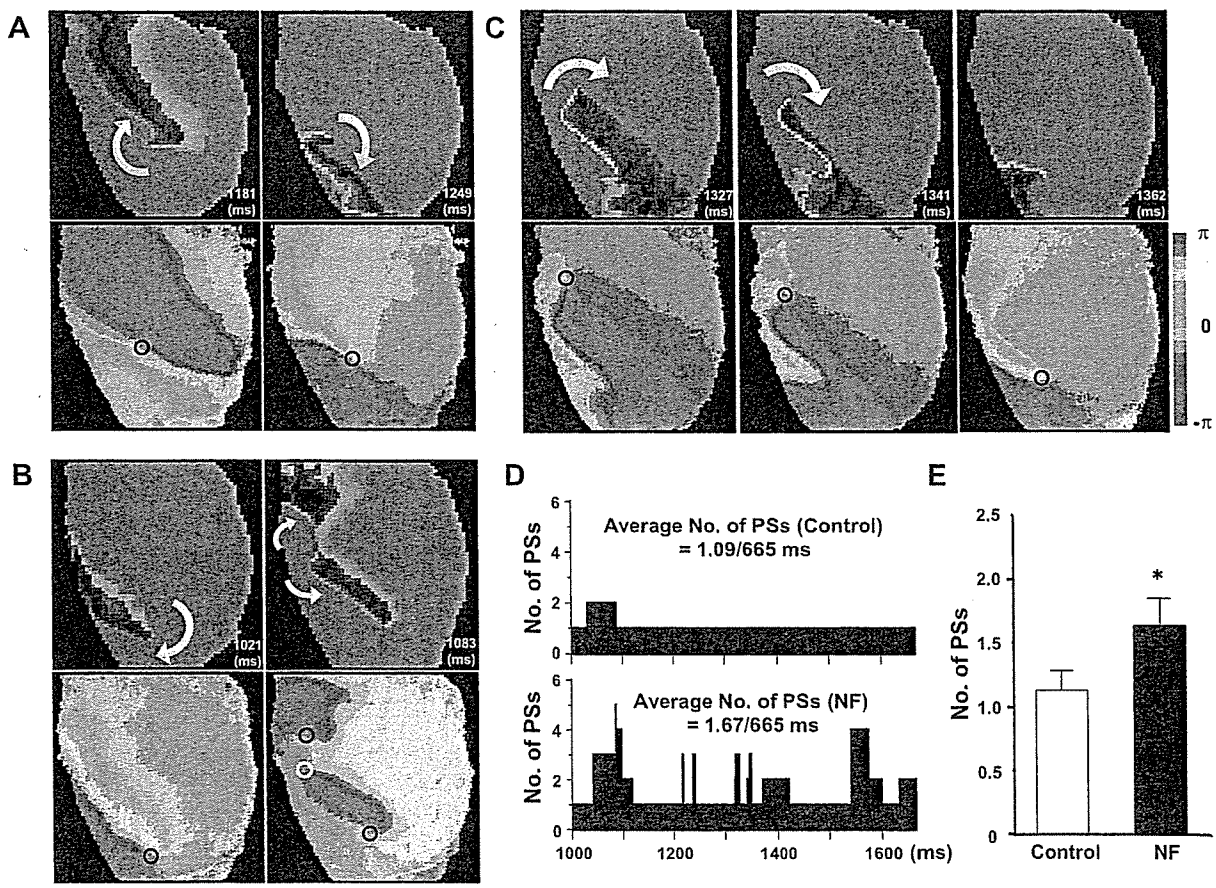

Fig. 3. Wave break formation by wave front-tail interaction. *A*: wave front (red) chasing a wave tail (green) during VT in the control condition. The *top* and *bottom* images are snapshots of wave front-tail and corresponding phase maps, respectively. The wave front does not encounter the tail (no breakup). *B*: interaction of a wave front with a wave tail during VT after application of 0.1 μM NF, causing the transient breakup of a rotor. *C*: interaction of a wave front with a wave tail during VT after NF, causing a sudden movement of the organizational center to another site. Phase singularity points (PSs) are indicated by circles (black for clockwise rotation, white for counterclockwise rotation). *D*: number of PSs over 500 frames (665 ms) during VT before (*top*) and after NF (*bottom*) (from the same heart as in *A–C*). *E*: average number of PSs/500 frames (665 ms) before (control) and after NF (means ± SD, $n = 7$). *$P < 0.05$ vs. control.

the average number of PS points during 500 frames (665 ms) was 1.13 ± 0.14 in the control and 1.63 ± 0.22 after NF (n = 7, $P < 0.05$).

Mode of spiral wave termination. The mode of spontaneous termination of spiral wave excitation was analyzed in 10 VT episodes in the absence of NF (control) and 19 VT episodes in the presence of NF. In the controls, most VTs (9/10, 90.0%) terminated as a result of mutual annihilation of counterrotating spiral waves. Figure 4*A* shows representative experiments (see Supplemental Movie 3). Excitation patterns for the final beat of a VT episode are shown in four sequential phase maps (*left*). A pair of PS points with opposite chiralities constructing a figure eight reentry circuit was present in the lower region of the left ventricle (1,850 ms). The distance between the two PS points initially increased (1,850 to 1,935 ms) and then decreased (1,935 to 1,951 ms), culminating in mutual annihilation (1,961 ms). The trajectories of the 2 PS points plotted on space (x, y) and time axes are shown in the *middle* (red, clockwise; blue, counterclockwise). Action potential signals recorded from six sites in the figure eight reentry circuit (*right*) revealed conduction block at the central common pathway (*site d*). In the remaining control episode, the VT ended by extinction of a single rotor when it collided against the anatomic boundary (atrioventricular groove).

In the presence of NF, 12/19 VTs (63.2%) terminated by rotor extinction after considerable meandering toward the anatomic boundary. Figure 4*B* shows an example (see Supplemental Movie 4). In the four sequential phase maps (*left*), a clockwise rotating PS initially moved a long distance from the upper right region to the right margin, then back toward the upper central region (1,282 to 1,382 ms), and was finally pushed out of the atrioventricular groove (1,463 to 1,490 ms). The trajectory of the PS plotted on space and time axes is shown in the *middle* (the blue wall at *right* indicates the atrioventricular groove), and action potential signals recorded from five sites in the meandering pathway are shown at *right*.

In the remaining seven VTs (36.8%) in the presence of NF, the rotors terminated by trapping the spiral tip in a region

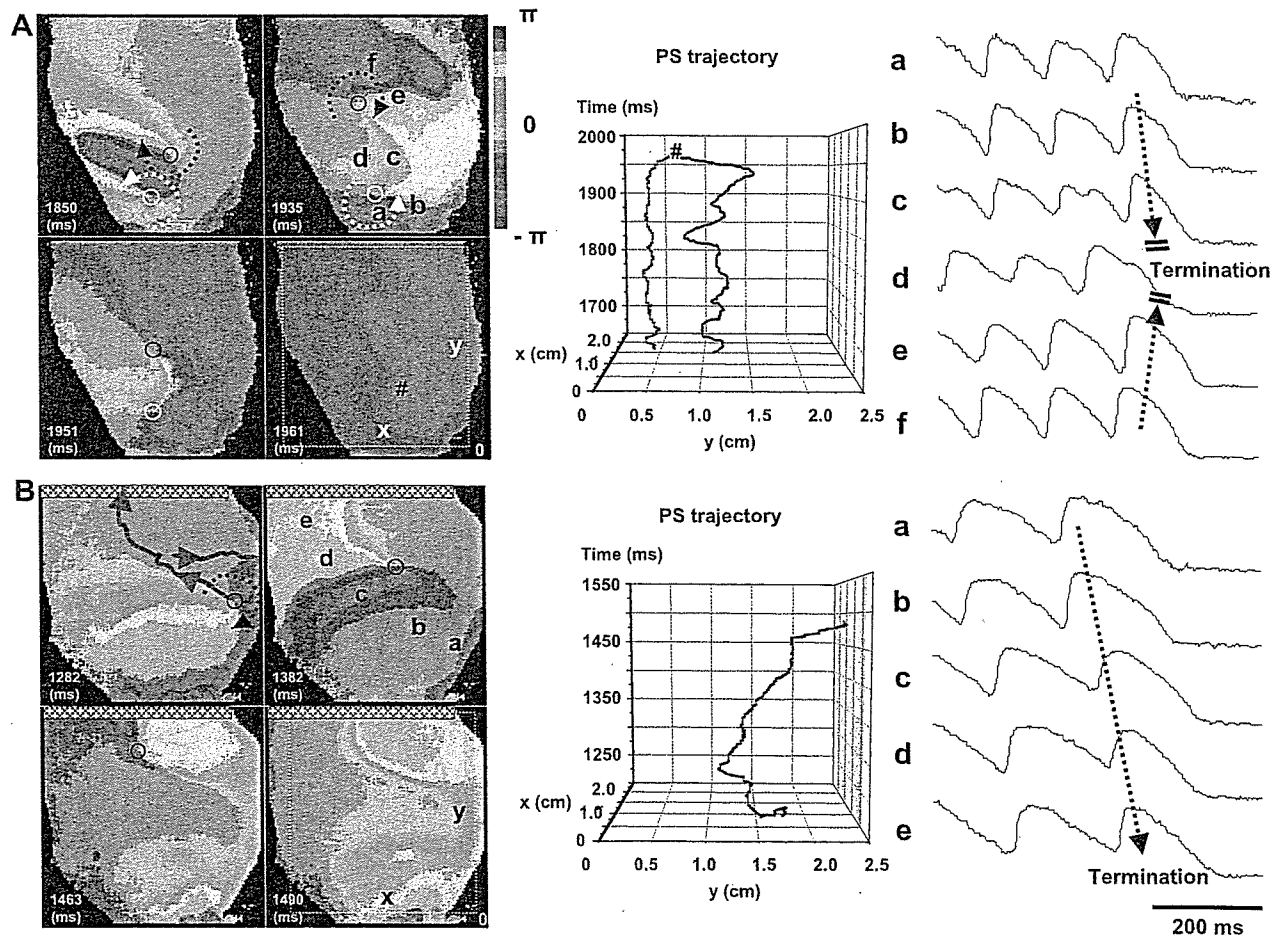

Fig. 4. Spiral wave reentry terminated by mutual annihilation and exit from the ventricles. *A*: spontaneous termination of VT in the absence of NF (control) as a result of mutual annihilation of counterrotating spiral waves (#). *Left*, 4 snapshots of phase maps of the final beat of a VT episode; PSs are indicated by circles (black for clockwise rotation, white for counterclockwise rotation). *Middle*, trajectories of the 2 PSs plotted on space (x, y) and time axes (red for clockwise rotation, blue for counterclockwise rotation). *Right*, optical action potential signals from 6 sites (*a–f*) indicated at *left*. *B*: spontaneous termination of VT in the presence of NF by exit of a rotor from the ventricles. *Left*, 4 snapshots of phase maps of the last beat; crosshatched bar at *top* of each frame indicates the atrioventricular groove, and red line indicates the trajectory of a PS. *Middle*, trajectory of a PS plotted on space (x, y) and time axes (blue wall at *right* indicates the atrioventricular groove). *Right*, optical action potential signals recorded from 5 sites (*a–e*) indicated at *left*.

entirely surrounded by refractory tissue. Figure 5 shows a representative experiment. Isochrone and APD_{90} maps of three beats before termination are shown in Fig. 5*A*. In *beat 1*, activation from the left upper region turned around a short functional block line (yellow) in a clockwise direction. In *beat 2*, the clockwise rotation was maintained and associated with extension of the functional block line toward the central region. In *beat 3*, the wave front from the left upper region was blocked in the central region. Because this wave front (red dotted line) was entirely surrounded by a refractory zone, no offspring wavelets emerged, and the VT terminated. Action potential signal tracings from two sites (asterisks) revealed APD alternans during the VT cycles (Fig. 5*B*), with the longest APD_{90} of *beat 3* (*site a*) preventing further rotation of the wave front. The APD maps of *beat 3* visualized trapping of the entire spiral tip by the long APD_{90} zone. A similar enhancement of APD alternans preceding the spontaneous termination was observed in all seven VTs of this group. Figure 5*C* shows phase maps of the final beat (see Supplemental Movie 5). The PS of clockwise rotation shifted from the left upper region to the center and then disappeared. The trajectory of the PS plotted on space and time axes is shown in Fig. 5*D*.

VTs induced in the absence of BDM. In three hearts, VTs were induced in the absence of BDM, and the effects of NF (0.1 μM) on the spiral wave dynamics were analyzed using phase maps. The results in each of the three hearts were essentially similar to those obtained in the presence of BDM. In controls, 27 of 32 VTs (84.4%) terminated spontaneously within 30 s (nonsustained), whereas the other 5 VTs (15.6%) persisted >30 s (sustained). Of these VTs, 26 (81.3%) terminated within 5 s. All 12 VTs (100%) in the presence of NF were nonsustained and terminated within 5 s.

A representative experiment is shown in Fig. 6. In the control conditions (Fig. 6*A*), a PS of counterclockwise rotation was present in the middle of the anterior surface of the left ventricle. A trajectory of the PS revealed that the rotor was more or less stable and exhibited moderate meandering (1,718–2,041 ms). After application of NF (Fig. 6*B*), a PS of clockwise rotation moved a long distance with a complex trajectory; from the right margin to the upper central region

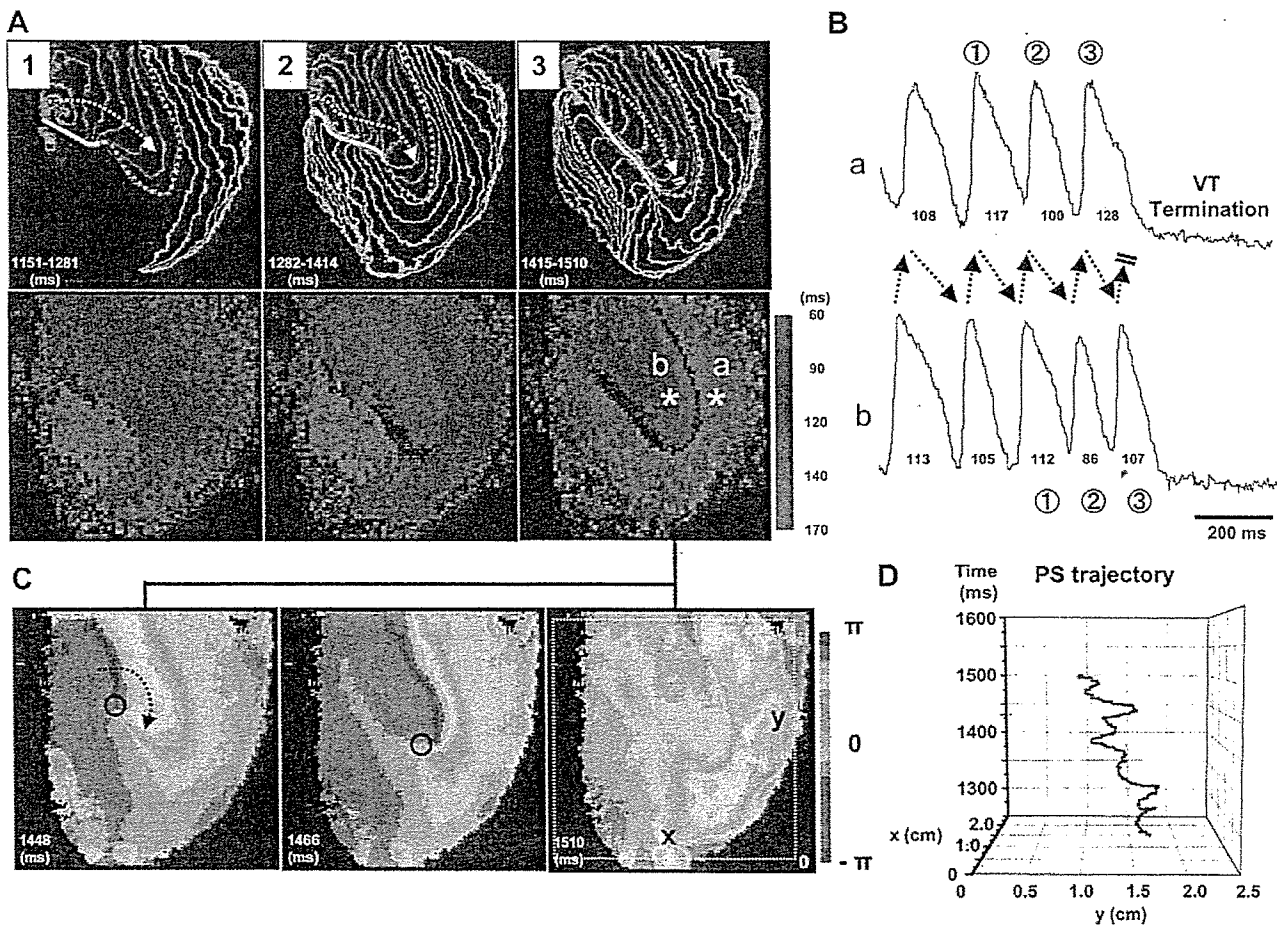

Fig. 5. Spiral wave reentry termination by trapping the wave front. *A*: isochrone and APD_{90} maps of the final 3 beats of VT before spontaneous termination in the presence of NF. Isochrones are at 5.33-ms intervals (green lines for earlier wave fronts, blue lines for later wave fronts). The latest activation front is presented by a dotted red line, and the line of functional block is shown in yellow. APD_{90} in the recording area is represented by color gradients, ranging from red (shortest) to blue (longest). *B*: optical action potential signals recorded at 2 sites (*sites a* and *b* in *A*). Numbers at the bottom of each action potential indicate the APD_{90} (ms). *C*: snapshots of phase maps in the final beat. PS with clockwise rotation is indicated by a black circle. *D*: trajectory of the PS plotted on space (x, y) and time axes.

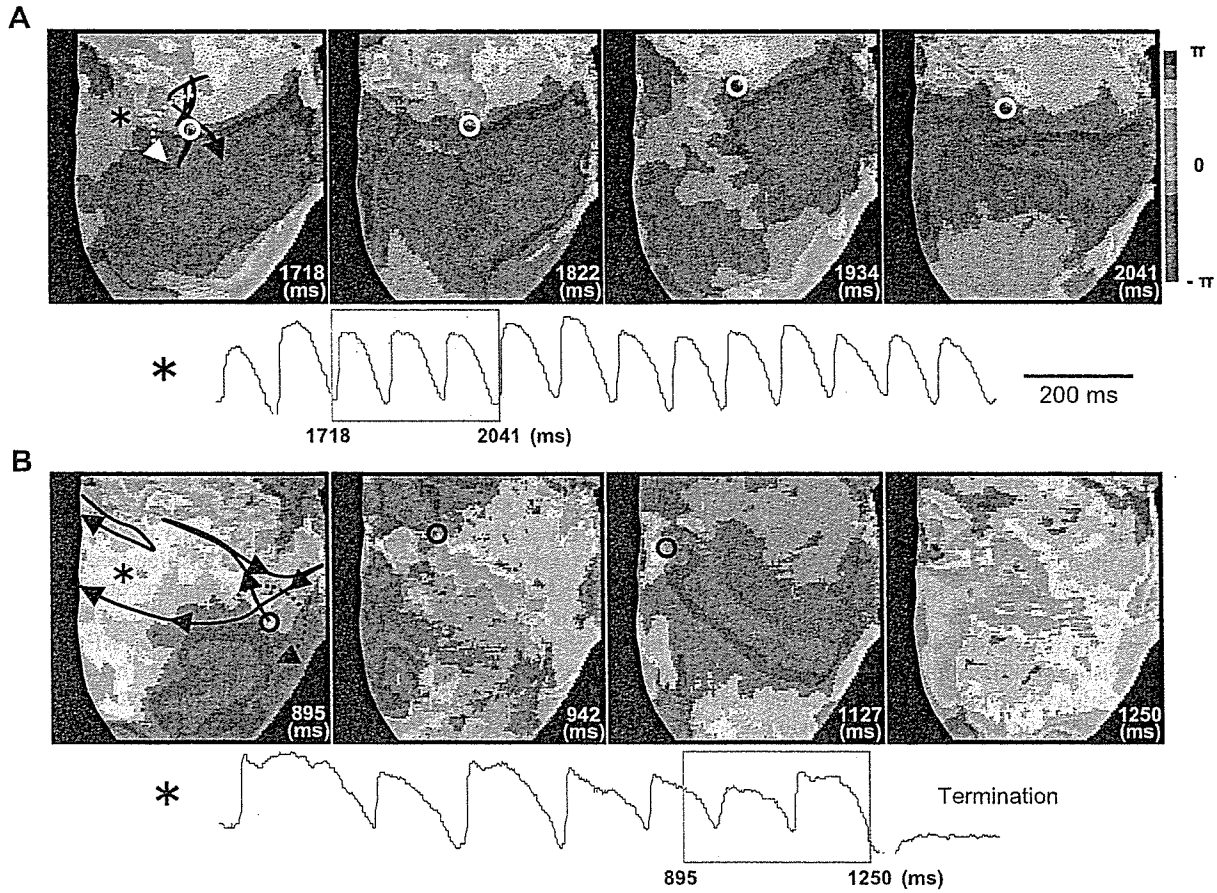

Fig. 6. Effects of NF on the spiral wave reentry dynamics in the absence of 2,3-butanedione monoxime (BDM). *A*: 4 snapshots of phase maps during a VT episode in the control condition. *B*: 4 snapshots of phase maps at the end (spontaneous termination) of a VT episode after NF (0.1 μM). PSs are indicated by white and black circles (counterclockwise and clockwise rotation, respectively); PS trajectory is indicated by solid lines. Optical action potential signals recorded from a left upper region (asterisk) are shown at *bottom*.

(895–942 ms), going back to the right margin, followed by a traverse in opposite direction toward the posterior surface. The PS reappeared on the anterior surface (left upper region), turned back toward the left upper corner (anatomical boundary), and terminated (1,127–1,250 ms). Action potential signals showed nearly uniform configuration in control (Fig. 6*A*) compared with marked beat-to-beat variation after NF (Fig. 6*B*).

DISCUSSION

The results of this study in a 2D ventricular myocardium with normal anisotropy have revealed that NF-induced delay and dynamic instability of ventricular repolarization causes frequent collision of spiral wave fronts with their own tails or anatomical boundaries, giving rise to breakup, sudden movement of PS, or extinction of rotors.

Action potential and conduction properties. In this study, we first examined the effects of 0.1 μM NF on the conduction velocity and APD under constant stimulation at a wider range of BCLs (180–800 ms) than in our previous study at 0.5 μM (BCLs 250 and 400 ms) (1). NF (0.1 μM) caused spatially uniform APD prolongation without affecting conduction velocities. The APD prolongation was significant even at a BCL of 180 ms, but it was greater at longer BCLs. The spatial dispersion of APD measured at 16 sites to cover an 18 × 18-mm square was unaffected by NF. NF increased the slope of the APD restitution curve, and the change was associated with an increase in APD alternans. All of these NF-induced alterations in the steady-state and dynamic electrophysiological properties of ventricular muscle can be ascribed to I_{Kr} blockade. In action potential clamp experiments, Hua and Gilmour (7) recently demonstrated that I_{Kr} contribute importantly to ventricular muscle repolarization during normal and high-frequency stimulation and that APD alternans is regulated substantially by time- and voltage-dependent activation and deactivation of I_{Kr}.

VTs of spiral wave reentry. In our 2D ventricular muscle tissue preparations of rabbit heart, spiral wave reentry rotating around functional block lines (single or double loops) can be induced by modified cross-field stimulation in the observation area in more than half (53–61%) of whole VT episodes under the control conditions (1, 10). The VTs induced are polymorphic during the initial several beats (1, 10) but become almost monomorphic during the subsequent beats. Microscopic structural discontinuities in association with anisotropic fiber orientation or epicardial blood vessels may provide a basis for this anchoring behavior.

VTs induced in the presence of NF (0.1 μM) are, consistent with our previous report with NF at 0.5 μM (1), characterized by longer cycle length, polymorphic configuration, and earlier termination than those observed in the controls. The optical images showed that these changes were associated with marked destabilization of rotors, which circulated around much longer and variable functional block lines formed by refractory wake of preceding excitations. We analyzed movies of wave front and wave tail during the rotations and found that a wave front in the presence of NF (0.1 μM) frequently encounters its own tail, resulting in breakup or sudden jump of organizational center of the rotation. The marked destabilization of rotors in the presence of NF cannot be ascribed to a APD restitution slope >1, since the maximum slope after NF, although increased, remained 0.7 on average. Other factors such as short-term cardiac memory, electronic currents, and unstable intracellular Ca^{2+} cycling also can affect wave stability and may have played a role in enhancing meander of the circuit. The enhanced meandering may have further facilitated the wave front-tail interactions through creation of Doppler-shifted short cycle length in front of moving phase singularities (4, 6).

Spiral wave reentry termination. Information on the effect of I_{Kr} block on the dynamics of spiral wave reentry in the ventricular myocardium is still limited. An analysis of computer model of isotropic 2D cardiac tissue showed discrepancies among investigators in the role of the delayed rectifier K^+ current (I_K) in the regulation of spiral wave dynamics. In their model, Beaumont and Jalife (2) showed that APD is significantly abbreviated (too short for I_K activation) near the center of the rotation. Thus I_K block prolongs APD only in the periphery and not close to the center. This leads to frequent wave front-tail interaction in the spiral arm without affecting the rotation period. Jalife and colleagues (2, 21) suggested that the inward rectifier K^+ current (I_{K1}) may play a much more important role than I_K [I_{Kr} and I_{Ks} (slow component)] in regulation of spiral core dynamics. In their simulation using the phase 1 Luo-Rudy ventricular action potential model, on the other hand, Qu et al. (18) have shown that APD close to the spiral core is longer than in the periphery and that a substantial amount of I_K is preserved at the rotation center. They demonstrated that reduction of I_K conductance promotes meandering of the spiral core and that quasiperiodic meandering is converted to chaotic meandering that culminates in the breakup of rotors (18).

Our observations in the rabbit heart suggest that I_{Kr} plays an essential role in repolarization of the action potential not only in the arm but close to the core of spiral wave reentry. In the absence of NF (control), most spontaneous terminations of spiral-type excitations were the result of mutual annihilation of a pair of rotors with opposite chiralities. NF facilitated the spontaneous termination by two different mechanisms: extinction of rotor(s) after collision with the anatomic boundary, and trapping of the spiral tip in a region entirely surrounded by refractory tissue. The former mode is attributable to considerable meandering of the rotation center, whereas the latter is attributable to APD prolongation of the preceding excitation in association with increased APD alternans near the spiral tip. The latter mode of termination is similar to that reported by Beaumont and Jalife (2) in their 2D cardiac tissue model when sodium current inactivation was slowed in combination with APD prolongation or when the outward component of I_{K1} was reduced. In a recent theoretical study by Qu and Weiss (19), blockade of time-dependent K^+ channel was shown to increase dynamic instability of rotors and to facilitate their self-termination. The present results validate their prediction.

Most of the modification of spiral wave dynamics induced by NF (0.1 μM) may be shared by other I_{Kr} blocking drugs, since much higher concentrations (5–100 μM) are required for NF to affect other voltage- and ligand-gated K^+ currents (17). However, further experimental studies are required to elucidate the point.

Limitations. In this study using a 2D subepicardial layer of rabbit ventricular myocardium, NF-induced delay and instability of ventricular repolarization were shown to cause frequent collision of spiral wave fronts with their own tails or anatomical boundaries, giving rise to breakup or early extinction of rotors. Extending these results to 3D hearts, especially in larger animals including humans, is not straightforward. If there is sufficient tissue mass, the chance of spontaneous termination of rotors by wave front collision or trapping would be reduced, whereas the enhancement or rotor meander and wave instability may promote breakup in favor of transition from VT to VF. The greater structural discontinuities and functional heterogeneities in diseased hearts would also alter the spatial requirements of spontaneous rotor termination. Thus NF can be not only antiarrhythmic but also proarrhythmic. There are certain clinical reports (in Japanese) showing excessive QT prolongation and torsades de pointes induced by NF (0.1–0.3 mg/kg iv). Plasma concentrations at such therapeutic doses are comparable to the NF concentration (0.1 μM) employed in the present study (17). The proarrhythmia via rotor breakup might be dangerous, since it would promote VF generation and perpetuation. We used BDM as an excitation-contraction uncoupler that is known to alter ionic currents and to reduce the APD restitution slope (13). However, this does not seem to invalidate the present results, because the characteristic modification of the spiral wave dynamics by NF was preserved in the absence of BDM. We cannot completely neglect the potential photodynamic toxicity of the voltage-sensitive dye (di-4-ANEPPS), but this may not have significant effects on the electrophysiological properties of the preparations in our experimental conditions, because there were no time-dependent changes of conduction velocity and action potential configuration up to 120 min of control perfusion (see Supplemental Table 1). There are considerable species differences in the relative contribution of I_{Kr} to the repolarization of action potential in ventricular myocytes. Despite these limitations, the present results may provide a new perspective for future development of drugs to prevent sudden arrhythmic death.

GRANTS

This study was supported by Grant-in-Aid for Scientific Research (A) 14207034 from the Japan Society for the Promotion of Science and by the Health and Labor Science Research on Medical Devices for Analyzing, Supporting and Substituting the Function of Human Body from the Ministry of Health, Labor and Welfare of Japan (H15–17 Physi-001).

REFERENCES

1. **Amino M, Yamazaki M, Nakagawa H, Honjo H, Okuno Y, Yoshioka K, Tanabe T, Yasui K, Lee JK, Horiba M, Kamiya K, Kodama I.** Combined effects of nifekalant and lidocaine on the spiral-type re-entry in a perfused 2-dimensional layer of rabbit ventricular myocardium. *Circ J* 65: 576–584, 2005.

2. **Beaumont J, Jalife J.** Rotors and spiral waves in two dimensions. In: *Cardiac Electrophysiology: From Cell to Bedside* (3rd ed.), edited by Zipes DP, Jalife J. Philadelphia, PA: Saunders, 2000, p. 327–335.
3. **Davidenko JM, Pertsov AM, Salomonsz R, Baxter WP, Jalife J.** Stationary and drifting spiral waves of excitation in isolated cardiac muscle. *Nature* 355: 349–351, 1992.
4. **Fenton FH, Cherry EM, Hastings HM, Evans SJ.** Multiple mechanisms of spiral wave breakup in a model of cardiac electrical activity. *Chaos* 12:852–892, 2002.
5. **Gray RA, Pertsov AM, Jalife J.** Spatial and temporal organization during cardiac fibrillation. *Nature* 392: 75–78, 1998.
6. **Gray RA, Jalife J, Panfilov AV, Baxter WT, Cabo C, Davidenko JM, Pertsov AM.** Mechanisms of cardiac fibrillation. *Science* 270: 1222–1223, 1995.
7. **Hua F, Gilmour RF Jr.** Contribution of I_{Kr} to rate-dependent action potential dynamics in canine endocardium. *Circ Res* 94: 810–819, 2004.
8. **Jalife J.** Ventricular fibrillation: mechanisms of initiation and maintenance. *Annu Rev Physiol* 62: 25–50, 2000.
9. **Kamiya J, Ishii M, Katakami T.** Antiarrhythmic effects of MS-551, a new class III antiarrhythmic agent, on canine models of ventricular arrhythmia. *Jpn J Pharmacol* 58: 107–115, 1992.
10. **Kodama I, Honjo H, Yamazaki M, Nakagawa H, Ishiguro Y, Okuno Y, Sakuma I, Kamiya K.** Optical imaging of spiral waves: pharmacological modification of spiral-type excitation in a 2-dimensional layer of ventricular myocardium. *J Electrocardiol* 38: 126–130, 2005.
11. **Koller ML, Riccio ML, Gilmour RF Jr.** Dynamic restitution of action potential duration during electrical alternans and ventricular fibrillation. *Am J Physiol Heart Circ Physiol* 275: H1635–H1642, 1998.
12. **Kushida S, Ogura T, Komuro I, Nakaya H.** Inhibitory effect on the class III antiarrhythmic drug nifekalant on HERG channels: mode of action. *Eur J Pharmacol* 457: 19–27, 2002.
13. **Lee MH, Lin SF, Ohara T, Omichi C, Okuyama Y, Chudin E, Garfinkel A, Weiss JN, Karagueuzian HS, Chen PS.** Effects of diacetyl monoxime and cytochalasin D on ventricular fibrillation in swine right ventricles. *Am J Physiol Heart Circ Physiol* 280: H2686–H2696, 2001.
14. **Murakawa Y, Yamashita T, Kanese Y, Omata M.** Can a class III antiarrhythmic drug improve electrical defibrillation efficacy during ventricular fibrillation? *J Am Coll Cardiol* 29: 688–692, 1997.
15. **Myoishi M, Yasuda S, Miyazaki S, Ueno K, Morii I, Satomi K, Otsuka Y, Kawamura A, Kurita T, Kitamura S, Nonogi H.** Intravenous administration of nifekalant hydrochloride for the prevention of ischemia-induced ventricular tachyarrhythmia in patients with renal failure undergoing hemodialysis. *Circ J* 67: 898–900, 2003.
16. **Nakaya H, Tohse N, Takeda Y, Kanno M.** Effects of MS-551, a new class III antiarrhythmic drug, on action potential and membrane currents in rabbit ventricular myocytes. *Br J Pharmacol* 109: 157–163, 1993.
17. **Nakaya H, Uemura H.** Electropharmacology of nifekalant, a new class III antiarrhythmic drug. *Cardiovasc Drug Rev* 16: 133–144, 1998.
18. **Qu Z, Xie F, Garfinkel A, Weiss JN.** Origins of spiral wave meander and break in a two-dimensional cardiac tissue model. *Ann Biomed Eng* 28: 755–771, 2000.
19. **Qu Z, Weiss JN.** Effects of Na^+ and K^+ channel blockade on vulnerability to and termination of fibrillation in simulated normal cardiac tissue. *Am J Physiol Heart Circ Physiol* 289: H1692–H1701, 2005.
20. **Roden DM.** Drug-induced prolongation of the QT interval. *N Engl J Med* 350:1013–1022, 2004.
21. **Samie FH, Berenfeld O, Anumonwo J, Mironov SF, Udassi S, Beaumont J, Taffet S, Pertsov AM, Jalife J.** Rectification of the background potassium current. A determinant of rotor dynamics in ventricular fibrillation. *Circ Res* 89: 1216–1233, 2001.
22. **Samie FH, Jalife J.** Mechanisms underlying ventricular tachycardia and its transition to ventricular fibrillation in the structurally normal heart. *Cardiovasc Res* 50: 242–250, 2001.
23. **Schalij MJ, Lammers WJEP, Rensma PL, Allessie MA.** Anisotropic conduction and reentry in perfused epicardium of rabbit ventricle. *Am J Physiol Heart Circ Physiol* 263: H1466–H1478, 1992.
24. **Takenaka K, Yasuda S, Miyazaki S, Kurita T, Sutani Y, Morii I, Daikoku S, Kamakura S, Nonogi H.** Initial experience with nifekalant hydrochloride (MS-551), a novel class III antiarrhythmic agent, in patients with acute extensive infarction and severe ventricular dysfunction. *Jpn Circ J* 65: 60–62, 2001.
25. **Weiss JN, Garfinkel A, Karagueuzian HS, Qu Z, Chen PS.** Chaos and the transition to ventricular fibrillation. A new approach to antiarrhythmic drug evaluation. *Circulation* 99: 2819–2826; 1999.
26. **Weiss JN, Qu Z, Chen PS, Lin SF, Karagueuzian HS, Hayashi H, Garfinkel A, Karma A.** The dynamics of cardiac fibrillation. *Circulation* 112: 1232–1240, 2005.
27. **Winfree AT.** Electrical turbulence in three-dimensional heart muscle. *Science* 266: 1003–1006, 1994.

表　題

著者名

醫學のあゆみ 別刷

第　巻・第　号：　　年　月　日号

薬物による心室スパイラル・リエントリーの制御
——高分解能光学マッピング実験による解析
Pharmacological regulation of spiral-wave reentry in the heart

児玉逸雄(写真)　本荘晴朗
Itsuo KODAMA[1] and Haruo HONJO[2]
名古屋大学環境医学研究所循環器分野[1]，同液性調節分野[2]

◎心室頻拍，心室細動(VT/VF)の成立には，渦巻き型の旋回興奮(スパイラル・リエントリー)が重要な役割を果たす．著者らは高分解能活動電位光学マッピングを用いた実験で，Na，Ca，K チャネルに対する遮断薬と，複数のチャネルやトランスポータに作用する薬物(アミオダロン)が動物の灌流心に誘発したスパイラル・リエントリーのダイナミックに及ぼす作用を検討した．Na チャネルや Ca チャネルだけを遮断する薬物はリエントリーを安定化させ，VT 持続を延長させる効果があった．遅延整流 K チャネルの速い活性化成分(I_{Kr})を遮断する薬物はスパイラルを不安定にし，分裂をもたらす一方で，その早期停止を促す作用があった．アミオダロンはスパイラルの分裂を減らしながら，その早期停止を促した．スパイラル・リエントリーの制御による VT/VF 治療には，脱分極と再分極の両者に対して多面的に作用する薬物が必要と考えられる．

Key word：スパイラル・リエントリー，光学マッピング，イオンチャネル遮断薬，アミオダロン

心室細動(VF)は血行動態の破綻をきたし，心臓突然死の主要な原因となることが知られている[1]．VF の多くは心室頻拍(VT)を契機として発症する．近年，これらの致命的な心室不整脈(VT/VF)の発生に渦巻き型の旋回興奮(スパイラル・リエントリー)が重要な役割を果たすことが示され，心臓突然死対策を考えるうえでの新しい概念として注目を集めている[2-5]．スパイラル・リエントリーは化学溶液中での発色反応(Belouzov-Zabotinsky reaction)や，非線形媒体を想定したコンピュータシミュレーションから提唱された概念であるが，膜電位感受性色素を用いた活動電位光学マッピング技術の進歩によって動物の摘出心臓でも観察できるようになった[2]．しかし，薬物による心室スパイラル・リエントリーの制御に関してはまだ解明されていない部分が多く，VF 予防薬開発に向けての研究はようやく端緒についたところである．

著者らは東京大学新領域創成科学研究科(佐久間一郎教授)との共同研究により CMOS(complementary metal-oxide semiconductor)型の撮像素子を搭載した高速ビデオカメラを用いた高分解能光

サイドメモ　スパイラル・リエントリー

機能的リエントリーのひとつであり，興奮波の形状が渦巻き型であることを特徴とする．興奮波が障害物にあたり端が切れることを発端として発生する．興奮前面が凸に彎曲した部分では既興奮部(上流)の未興奮部(下流)に対する割合が小さくなり，興奮前面で発生する局所電流の電流密度が減少するため，伝導速度が低下する．興奮波の端の部分では強い彎曲効果のため伝導速度が 0 となり(特異点)，この特異点を中心として旋回運動が持続する．スパイラル・リエントリーのダイナミクスは興奮媒体の特性によって変化する．媒体の興奮性が低い場合は旋回の中心は安定した円形の軌跡を描き，興奮波はその中(core)へ進入することができない．興奮性が高くなると，旋回中心は媒体の不応期に沿って移動し(さまよい運動，meandering)線状の機能的ブロック(functional block line：FBL)の周囲を旋回するようになる．

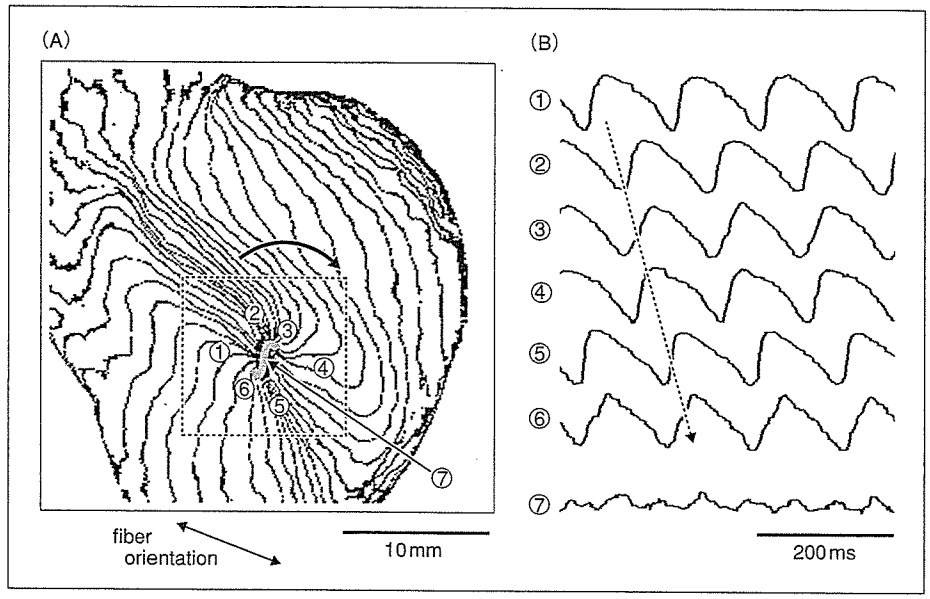

図 1　ウサギ心室の二次元灌流標本に直交電場刺激(cross-field stimulation)で誘発したスパイラル・リエントリー(薬剤添加前)
A：興奮到達の等時線図(4 ms 間隔)．B：旋回経路の 7 カ所(①～⑦)から記録した活動電位シグナル．

学マッピングシステムを開発し，この装置を用いて心室スパイラル・リエントリーのダイナミクスから薬物による修飾様式を検討する実験を行ってきた[6-9]．

本稿ではそれらの結果を紹介するとともに，理想的な抗細動薬に求められる条件について考えてみたい．

心室筋二次元灌流標本

心室壁には厚みがあるため，そこに発生したスパイラル・リエントリーは三次元構造(スクロール)をとり，リボン状の旋回中心(フィラメント)が複雑に変化する[10]．このため，心表面にはスパイラル構造は一瞬現れるが，不安定であり，すぐに他の興奮伝播様式に変化する．著者らはウサギの左室心内膜側を凍結凝固し，厚さ約 1 mm の心外膜下心筋だけを残存させた二次元灌流標本を作製した．この標本を膜電位感受性色素 di-4-ANEPPS で染色し，励起光照射で得られた螢光シグナルによる活動電位マッピングを行った．心筋収縮によるシグナル変動を除外するため，興奮収縮連関の脱共役剤(2,3-butanedione monoxime：BDM)を用いた．

標本の左室前面に刺激電極をおいて基本刺激(BCL 200～800 ms)を与えると，心筋線維に沿った方向に長軸をもつ左右対称の楕円形の興奮伝播が観察され，均一な異方性伝導(anisotropic conduction)[11]が確かめられた．長軸方向と短軸方向の伝導速度比は 2.9～3.1 であった．

心室頻拍の誘発とスパイラル・リエントリー

心室頻拍(VT)を誘発する実験では，心尖部からの基本刺激(S1-S1)による興奮に対して直交する方向に単相波電場刺激(S2，20 V，10 ms)を心室受攻期に与えた(cross field stimulation)[12]．左室前面と右室の一部を含む領域の螢光シグナルを高速ビデオカメラで撮影し，VT 中の興奮様式を観察すると 53%(61/116 VT)で観察領域にスパイラル構造を認めた(単一ループまたは 8 字形)．残り 47%では，興奮波が観察域を一方向に横切るパターンが主体であった．

VT 中に単一ループのスパイラル・リエントリーが観察された実験例の興奮等時線図(isochrone

map)と旋回経路の活動電位シグナルを図1に示す．左室前面のほぼ中央に線状の機能的ブロック(2.4 mm)が形成され，その周囲を興奮波が時計方向に旋回した(VTCL 115～118 ms)．機能的ブロックライン(FBL)は2つの部分から成り立っており，中央のセグメントはその両側で興奮の位相が大きく異なっていた(phase shift)．一方，FBL両端では等時線が重なっており，局所的な伝導遅延があった．後者の伝導遅延を伴うFBLは心筋線維に沿う方向に形成された．一方，前者のphase-shiftを伴うFBLは線維走行と無関係に形成された．旋回は小さなさまよい運動(meandering)を示しながら比較的安定した位置に数秒間以上とどまることが多かった．旋回経路の活動電位シグナルをみると，いずれも活動電位の再分極途中からつぎの活動電位が発生しており，連続する活動電位の電気的拡張期(electrical diastole)がほとんどない形をしている．FBLの端で興奮伝導の方向が急に変わる部分(旋回点：pivot point)では活動電位の立ち上りが他の部分よりも緩やかである．FBLの中央部では幅1～2 mmにわたった低振幅の二峰性電位(double potential)が記録された．

二次元構造をとる心室筋で発生するスパイラル・リエントリーは，Allessieら[13]がリーディングサークル説で提唱した機能的リエントリーの特徴(興奮波の前面がその終末部を最短の間隔で追いかける)と，異方性伝導(anisotropic conduction)[11]の特徴を兼ね備えた形で成立しており，興奮前面の彎曲効果(curvature effect)[14]がそれを修飾していることがわかる．リエントリー興奮波が向きを変えるpivot point付近では興奮前面の彎曲度(curvature)が強まり，既興奮部位から未興奮部位へと向かう局所電流密度が低下して興奮伝導効率が低下する(source/sink mismatch)．興奮伝導の方向が電気的結合の弱いT伝導から結合の強いL伝導に変わる部位では局所電流の多くが興奮の下流(sink)へ急速にながれこむことになり，当該部位の活動電位立ち上がり速度が低下すると考えられる[15]．

Naチャネル遮断薬の効果

Naチャネル遮断薬のpilsicainide(5 μM)は基本刺激下の伝導速度を30～40%低下させたが，活動電位持続時間(APD)は変化させなかった．図2-Aはpilsicainide作用下で誘発した単一スパイラル興奮を示す．興奮波は左室前面のFBLの周囲を時計方向に旋回しているが，コントロールに比べてFBLの両端の部分が大幅に延長している．VTCLは205～210 msへと延長し，このVTは30 s以上持続した．旋回経路の活動電位波形をみると，pivot point付近の活動電位の立ち上りが極端に緩やかになるとともに，興奮波がpivot pointをターンした後の活動電位に明らかな電気的拡張期(electrical diastole)が出現した．Disopyramide(30 μM)とcibenzoline(3 μM)を用いた実験でもpilsicainideに類似した効果が得られた．

Naチャネル遮断薬に共通するスパイラル・リエントリーの修飾作用は以下の4点に集約できる．①FBLの両端にある局所伝導遅延を増強し，旋回経路を拡大する(興奮前面が大きな波面を形成して方向転換する)．②Pivot pointをターンした後の活動電位に電気的拡張期(興奮間隙)が出現する．③リエントリー周期(VTCL)が延長する．④スパイラル・リエントリーが安定化する(VT持続時間の延長)．

Caチャネル遮断薬の効果

L型Caチャネル($I_{Ca,L}$)遮断薬の効果はベラパミル(3 μM)を用いた実験で検討した．ベラパミルは基本刺激下の伝導速度には影響を及ぼすことなく，APDを軽度短縮させた．ベラパミル作用下で誘発したスパイラル・リエントリーはFBLが短縮し，旋回経路が短くなりVTCLが短縮した．スパイラルのさまよい運動(meandering)は小さくなり，安定化して，VT持続時間が延長した．

Kチャネル遮断薬の効果

Kチャネル遮断薬としては，遅延整流K電流の速い活性化成分(I_{Kr})に対する選択的な遮断作用をもつnifekalant[16]の効果を検討した．Nifekalant(0.1～0.5 μM)は基本刺激下の伝導速度に影響を及ぼすことなくAPDを7～25%延長させた．Cross field stimulationで誘発したVT周期は延長したが，持続時間は短縮した(30s以上持続する

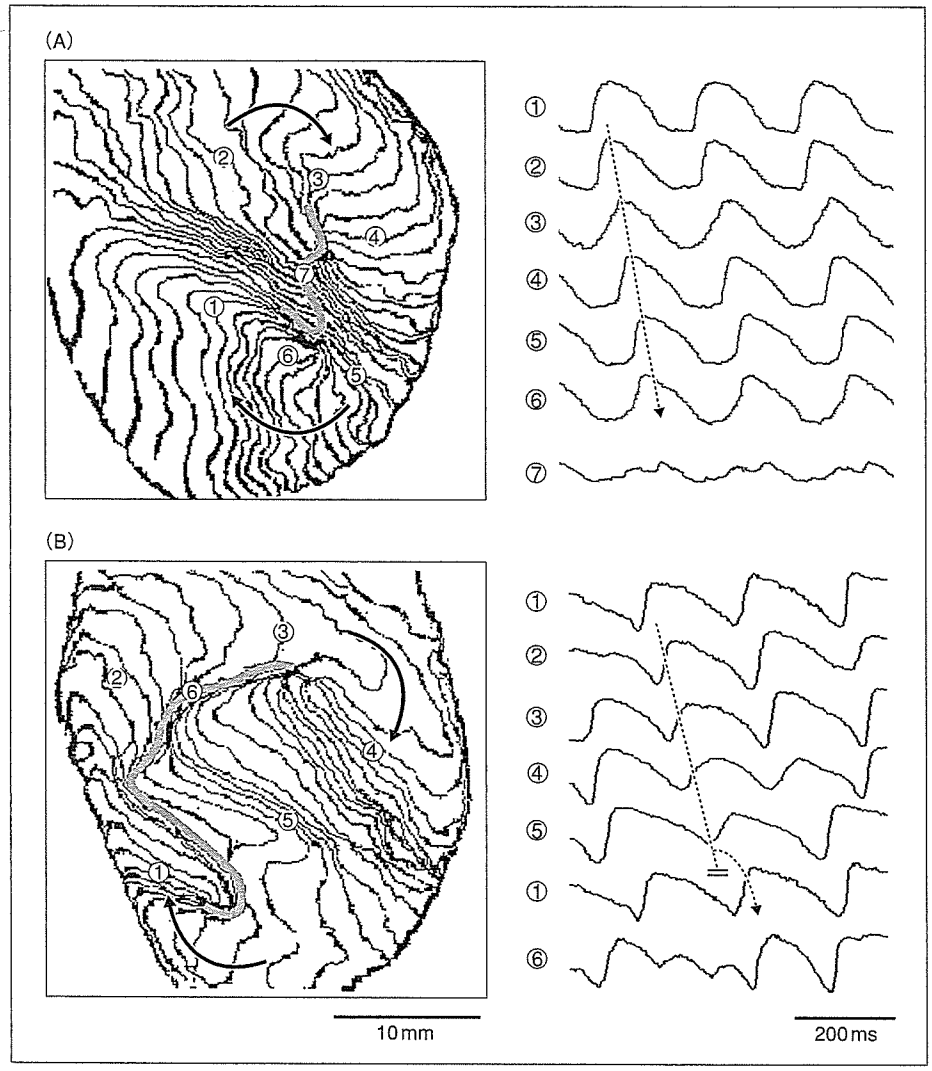

図 2　Naチャネル遮断薬とKチャネル(I_{Kr})遮断薬がスパイラル・リエントリーに及ぼす作用
A：Pilsicainide(5 μM)作用下で誘発した VT 中の興奮伝播過程．左は興奮到達の等時線図(4 ms 間隔)．右は旋回経路の 7 カ所(①～⑦)から記録した活動電位シグナル．B：Nifekalant(0.1 μM)作用下で誘発した VT 中の興奮伝播過程．左は興奮到達の等時線図(4 ms 間隔)．右は旋回経路の 6 カ所(①～⑥)から記録した活動電位シグナル．

VT の発生頻度は 25%から 10%に減少)．

図 2-B は nifekalant(0.1 μM)作用下で誘発した VT 中の(持続 3 s)興奮パターンを示す．興奮波は極端に延長し曲がりくねった FBL の周囲を旋回し，旋回経路は大きく不規則な meandering を示すようになった[9,17]．FBL の形状も一拍ごとに変化した．これは興奮波の前面(wave front)と興奮終末(wave tail)の衝突が頻繁に発生し，興奮波面の分裂や，旋回中心の突然の移動が起こることに起因している．旋回経路も一拍ごとに変化し，しばしば局所伝導ブロックが生じた[9,17]．このようなスパイラル・リエントリーの不安定化は I_{Kr}遮断作用によって心室全体の再分極遅延が生じ，旋回中の興奮可能領域が相対的に制限されたことによると考えられる．

アミオダロンの効果

アミオダロンは急性効果としては Na チャネル，Ca チャネル，K チャネル(とくに I_{Kr})遮断作用があり，そのほかのイオンチャネル，トランス

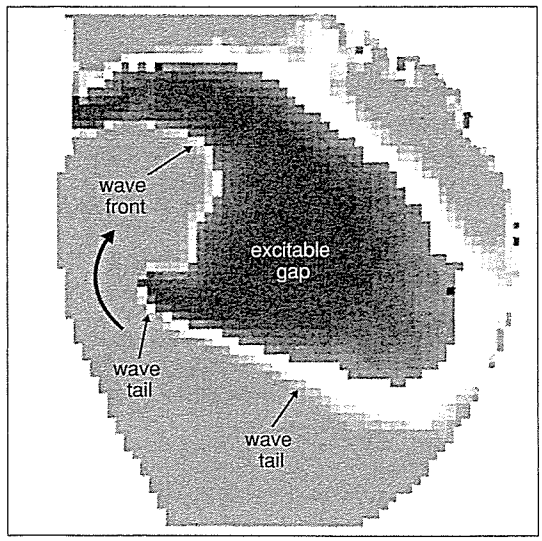

図3 スパイラル・リエントリー中の興奮前面(wave front)と興奮終末部(wave tail)の相互作用
Amiodarone(5 μM)作用下では wave front と wave tail の距離(excitable gap)が広がり，wave front と tail が衝突して興奮波面が分裂する(wave break)現象が減る．

ポータの機能にも複雑な影響を与えることが知られている[18]．

二次元灌流心室筋標本ではアミオダロン(5 μM)添加により伝導速度は6～15%低下し，APDは軽度(5～12%)延長した．Cross-field stimulationで誘発したVTCLは約25%延長したが，VT持続時間は短縮した(30s以上の sustained VT 発生頻度は30%から4%へ減少)．アミオダロン作用下で誘発したスパイラル・リエントリーは旋回中の興奮波の前面(wave front)と，それ自身の終末部(wave tail)の距離(spatial excitable gap)が広くなり，wave front が wave tail に追いついて波面が分裂する現象(wave break)が少なくなった[19](図3)．

スパイラル制御による心室細動防止薬

スパイラル・リエントリーが心室細動の成立にどのようにかかわるかについては，現在2つの考え方がある(mother rotor 仮説と dynamic wave break 仮説)[4,20,21]．Mother rotor 仮説では，心室の一部(不応期の短い部分)に限られた数の速い回転を示す rotor(エンジン)が存在し，ここから周囲の領域に興奮が不規則に伝播すること(fibrillatory conduction)が本体であると考えられている．一方，dynamic wave break(あるいは continuous wave break 仮説)では興奮波の分裂によって端の切れた波面が自己増殖的に繰り返し起こることが細動の本体であり，mother rotor の存在はかならずしも必要ないとされている．最近ではこれらの2つの概念は相反するものではなく相補的であり，病態や心筋組織の状態によって両者の寄与が異なるとする考え方が主流となってきた[21]．

著者らが二次元灌流心で得た薬物作用の実験結果から，Na チャネル遮断薬はスパイラルの旋回経路を大きくするとともに，興奮間隙を増してリエントリーを安定化させる作用があることが判明した．したがって，二次元構造をとるスパイラルであればその回転速度は低下し，mother rotor から発生する fibrillatory conduction は抑制されるはずである．心房細動に対する Na チャネル遮断薬の効果の一部はこのようなメカニズムで説明できるであろう．しかし，心室壁には厚みがあり，スパイラルは実際には三次元構造(スクロール)をしており，その旋回中心はリボン状のフィラメントとなっている．Na チャネル遮断薬による興奮性の低下はスクロール構造を不安定にし，興奮波面の分裂を促す作用がある．

Ca チャネル遮断薬に関しては，スパイラルを安定化させ，その旋回速度を増す作用がある．このため mother rotor の存続を促し，fibrillatory conduction を悪化させる可能性がある．

I_{Kr}チャネル遮断薬(nifekalant)はスパイラルを不安定にして，その成立を妨げる作用がある．したがって，mother rotor を基盤とする細動には，ある程度の停止効果，予防効果が期待できる．DC shock に抵抗性の心室細動は直流通電自体が仮想電極効果によってあらたなスパイラル・リエントリーを誘発し，それが虚血部位などの解剖学的な不連続部位に定在化(pinning)することが除細動不成功の主要な原因と考えられている[22]．I_{Kr}チャネル遮断薬によるスパイラル・リエントリーの不定在化(unpinning)は DC shock の成功率を上げる機序のひとつであろう．ただし，I_{Kr}作用下では興奮波面がそれ自身の終末部と相互に作用する機会が増して(wave front-tail interaction)，興奮波面の分

裂(wave break)を促すことで頻拍(VT)が細動(VF)に移行しやすくなる．これは dynamic break を基盤とする細動を悪化させる効果がある．

したがって，VF による心臓突然死を予防する観点からは，Na チャネル遮断薬，Ca チャネル遮断薬，I_{Kr}遮断薬はいずれも理想的な薬物とはいいがたい．アミオダロンは二次元灌流心におけるスパイラル興奮の break up を防ぎ，rotor を早期に停止させる効果がある．この効果がどのような分子標的を介する作用であるのか，三次元構造の心室でも同様な効果があるのかについてはいまのところ不明であり，今後の検討課題である．スパイラル興奮の分裂をもたらすことなく，その早期停止を促す薬物を探索することで，理想的な心室細動予防薬を開発するための重要な手がかりが得られることが期待される．

文献

1) Zipes, D. P. et al.：*Circulation*, **98**：2334-2351, 1998.
2) Davidenko, J. M.：Cardiac Electrophysiology：From Cell to Bedside. 2nd ed.(ed. by Zeipes, D. P. and Jalife, J.), W. B. Saunders, Philadelphia, 1997, pp.478-488.
3) Jalife, J.：*Ann. Rev. Physiol.*, **62**：25-50, 2000.
4) Samie, F. H. et al.：*Cardiovasc. Res.*, **50**：242-250, 2001.
5) Jalife, J. et al.：*Cardiovasc. Res.*, **54**：204-216, 2002.
6) 佐久間一郎・他：心臓, **33**：439-448, 2001.
7) 本荘晴朗・他：心臓, **33**：449-455, 2001.
8) 児玉逸雄・他：心臓, **34**：918-925, 2002.
9) Amino, M. et al.：*Circ. J.*, **69**：576-584, 2005.
10) Pertsov, A. M.：Cardiac Electrophysiology：From Cell to Bedside. 4th ed.(ed. by Zeipes, D. P. and Jalife, J.), W. B. Saunders, Philadelphia, 2004, pp.345-354.
11) Spach, M. S. et al.：Cardiac Electrophysiology：From Cell to Bedside. 3rd ed(ed. by Zeipes, D. P. and Jalife, J.), W. B. Saunders, Philadelphia, 2000, pp.213-222.
12) Frazier, D. W. et al.：*J. Clin. Invest.*, **83**：1039-1052, 1989.
13) Allessie, M. A. et al.：*Circ. Res.*, **41**：9-18, 1977.
14) Fast, V. G. et al.：*Cardiovasc. Res.*, **33**：258-271, 1997.
15) Schalij, M. J. et al.：*Circulation*, **102**：2650-2658, 2000.
16) Nakaya, H. et al.：*Cardiovasc. Drug. Rev.*, **16**：133-144, 1998.
17) Yamazaki, M. et al.：*Heart Rhythm*, **1S**：S255, 2004.
18) Kodama, I. et al.：*Cardiovasc. Res.*, **35**：13-29, 1997.
19) Nakagawa, H. et al.：*Heart Rhythm*, **1S**：S222, 2004.
20) Weiss, J. N. et al.：*Circ. Res.*, **87**：1103-1107, 2000.
21) Chen, P. S. et al.：*Circulation*, **108**：2298-2303, 2003.
22) Cheng, Y. et al.：*Circ. Res.*, **85**：1056-1066, 1999.

*　　*　　*